Influence of Solar Activity Cycles on Earth's Climate

ESA ITT AO/1-4618/NL/AR

Task 5 – Hypothetical Physical Mechanism

WP 502 – Solar wind interaction with magnetosphere and ionosphere

Technical Note

P. Wintoft and H. Lundstedt
Swedish Institute of Space Physics

26 March 2007

Document status sheet

ISSUE	REVISION	DATE	REASON FOR CHANGE
0	1	15 June 2006	First working draft.
0	2	12 September 2006	Updated draft.
0	3	26 March 2006	Updated draft. Changed rev. num.: starts at 1 instead of 0.

Contents

1 Introduction **1**

2 Large scale solar structures driving the solar wind **1**

3 The solar wind at 1 AU **2**

4 Magnetosphere **3**

5 Ionosphere **6**

6 Time scales of variability **11**

6.1 Solar wind 11

6.2 Magnetospheric activity 11

6.3 Coupling between systems 11

1 Introduction

The Sun is not in static equilibrium with the interstellar space. The high temperature in the corona together with the low pressure in interstellar space creates a continuous outflow of ionised gas called the solar wind. The solar wind is a plasma as

$$\lambda_D \propto \left(\frac{T}{n}\right)^{1/2} << L \tag{1}$$

$$N_D = \pi n^{4/3} \lambda_D^3 >> 1 \tag{2}$$

$$\frac{\omega_p}{\omega_c} > 1 \tag{3}$$

where λ_D is the Debye length, L is the size of the system studied, N_D the number of particles in the Debye sphere, ω_p is the plasma frequency, and ω_c is the collision frequency. From the induction equation

$$\frac{\partial \mathbf{B}}{\partial t} = \nabla \times (\mathbf{V} \times \mathbf{B}) + \eta \nabla^2 \mathbf{B} \tag{4}$$

and because the magnetic diffusivity $\eta = 1/(\mu\sigma) \approx 0$ as the electrical conductivity $\sigma \to \infty$ it follows that the magnetic fields and plasma moves together, a state called "frozen in". As a consequence the solar wind contains both plasma and magnetic fields. Typical values at Earth orbit (1 AU) are a velocity $V = 400$ km/s, particle density $n = 7$ cm^{-3}, and magnetic field strength $B = 5$ nT.

Several text books and review papers covers the solar wind, geomagnetic and iononospheric activity, just to mention a few: *Baumjohann and Haerendel* (1987); *Hargreaves* (1992); *Burlaga* (1995); *Lockwood* (2005).

2 Large scale solar structures driving the solar wind

At large scales the structures at the Sun driving the solar wind can be divided into to three classes that are all controlled by the solar magnetic fields. The coronal holes consist of open magnetic fields, basically directed radially inwards or outwards, causing a laminar high-speed low-density wind. Over active regions, such as sunspot groups, the magnetic fields are closed and more efficiently trapping the plasma causing a turbulent low-speed medium-density wind called coronal streamers. The coronal neutral line at 2–3 solar radii, computed from magnetostatic models (*Zhao and Hoeksema*, 1993), outlines the photospheric active regions and marks the transition from inward to outward (and vice verse) coronal hole magnetic fields. Figure 1 shows an example from March–April 2006. The large scale fields can persist for several solar rotations so that coronal holes and streamers are repeated with a 27 day period.

The third class is the coronal mass ejection (CME). The CME is a transient phenomena in which energy is released ejecting plasma and magnetic field over several solar radii during a few hours. Sometimes, but not always, the CME is simultaneous with a solar flare. The sites of the CMEs follow the coronal neutral line so that at sunspot minimum the CMEs occur along the solar equator while at sunspot maximum the CMEs can occur at high solar latitudes.

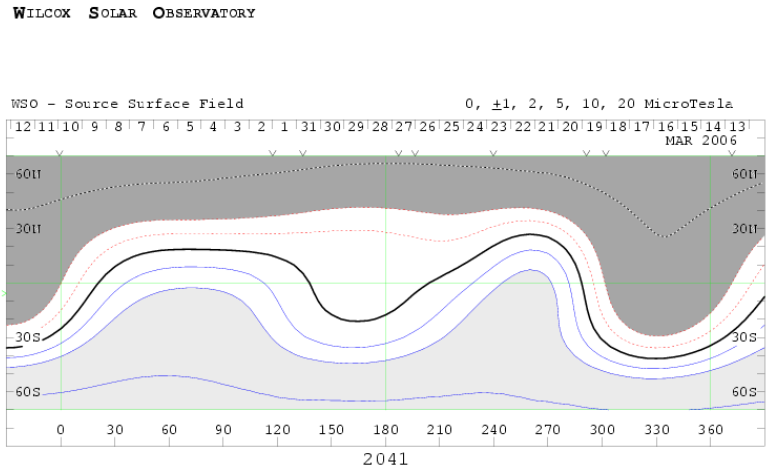

Figure 1: The computed magnetic field at 2.5 solar radii for the period 14 March to 10 April 2006. The black curve is the coronal neutral line. Blue solid curves marks the contour levels at 1, 2, and 5 μT (outward directed fields). Dotted red curves marks the contour levels at -1, -2, and -5 μT (inward directed fields). Image from `http://wso.stanford.edu/synsource.html`.

3 The solar wind at 1 AU

It takes typically $1.5 \cdot 10^8/400$ s = 375000 s = 4.3 days for the solar wind to travel from the Sun to Earth. However, CMEs may travel with a velocity of over 1000 km/s giving a travel time of 1.7 days or less. The velocity above coronal streamers may go below 300 km/s giving a travel time of more than 5.8 days. This variable time lag must be accounted for when relating solar phenomena with the solar wind or magnetosspheric and ionospheric activity with a temporal resolution of days. The lag plays a minor role for averages longer than 27 days.

Around sunspot number minimum the coronal neutral line is close to the solar equator and the ecliptic plane. Therefore, there will be no clear periodic pattern in the solar wind and in Figure 2 the velocity, particle density, and magnetic field are shown for a 90 day period starting on 1 April 1996, covering 3 solar rotations. The geomagnetic index Kp is also shown. The average Kp for the period is 1.65 and the correlation with velocity is 0.62.

Emanating from the coronal holes we have the high speed solar wind with typical velocity of 600–700 km/s. The temporal evolution of the solar wind over a 90 day period staring on 1 April 1995 is shown in Figure 3. This period was chosen as it occurs during the declining phase of solar cycle 21 when coronal holes dominates. The sunward component B_x of the magnetic field shows a bimodal distribution and is basically negative (pointing away from the Sun) for several days then changes sign (towards the Sun) for another extended period. This pattern is repeated for several rotations. We also see the increased particle densities simultaneous with the turning of the magnetic field associated with co-rotating interaction regions. When the coronal neutral line is far enough from

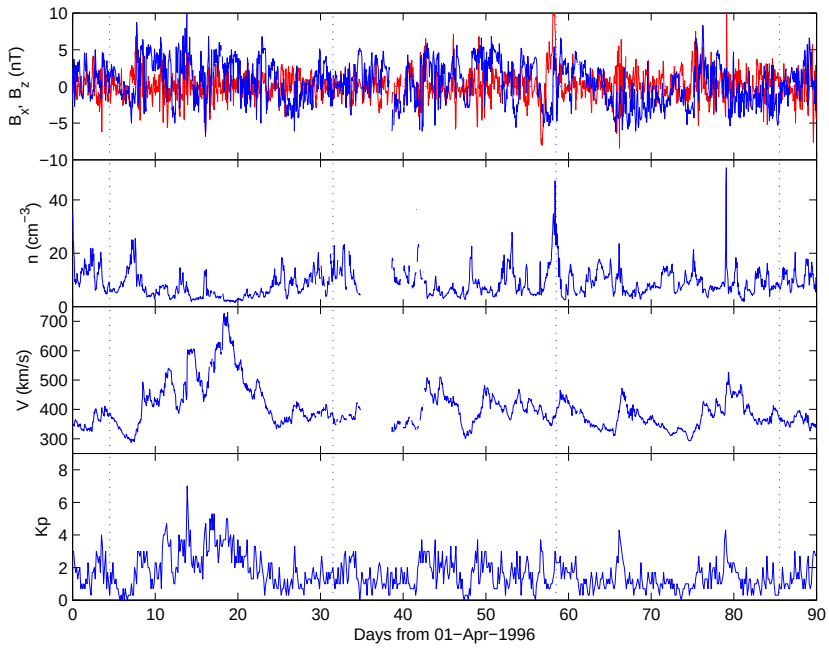

Figure 2: The solar wind magnetic field B_x (sunward component) in blue and B_z (out of the ecliptic) in red, particle density n, and velocity V during 90 days in 1996. The geomagnetic index Kp is also shown in the bottom panel. The vertical dotted lines are separated by 27 days.

the Sun–Earth line the velocity may take on high values as seen at days 7, 32, and 59. It also seen that V and Kp are correlated (corr.=0.64). The average Kp for the period is 2.39.

The CME produces a very different structure in the solar wind. In Figure 4 the solar wind data and Kp are shown for a 9-day period in April 2000. The velocity increases abruptly from 370 km/s to 560 km/s in less than an hour in the afternoon of the 6th. This is simultaneous with the southward turning of B_z and the increase in particle density n. Kp goes above 8 during 9 hours. We will discuss the coupling from the solar wind to geomagnetic activity in later sections.

4 Magnetosphere

The interaction between the solar wind and the Earth geomagnetic field creates the magnetosphere which is illustrated in Figure 5. As the plasma and magnetic fields obeys the frozen-in condition the solar wind and the magnetosphere forms to a first approximation two separate regions. The boundary is called the magnetopause and outside it there is a disturbed region called the magnetosheath out to the bow shock. The shape of the magnetosphere is then determined from the solar wind dynamic pressure and magnetic pressure

$$p = p_{\text{dyn}} + p_{\text{mag}} = mnV^2 + \frac{B^2}{\mu} \tag{5}$$

where m is the particle mass and μ is the magnetic permeability. Typical values in the solar wind are $p_{\text{dyn}} = 2 \cdot 10^{-9}$ Pa and $p_{\text{mag}} = 2 \cdot 10^{-11}$ Pa. With increased density, velocity, and/or

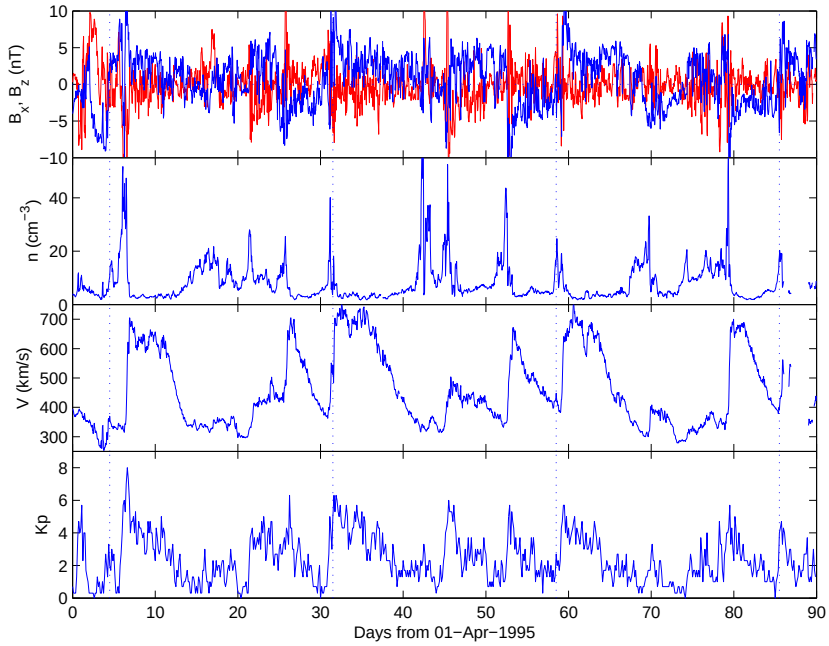

Figure 3: The solar wind magnetic field B_x (sunward component) in blue and B_z (out of the ecliptic) in red, particle density n, and velocity V during 90 days in 1995. The geomagnetic index Kp is also shown in the bottom panel. The vertical dotted lines are separated by 27 days.

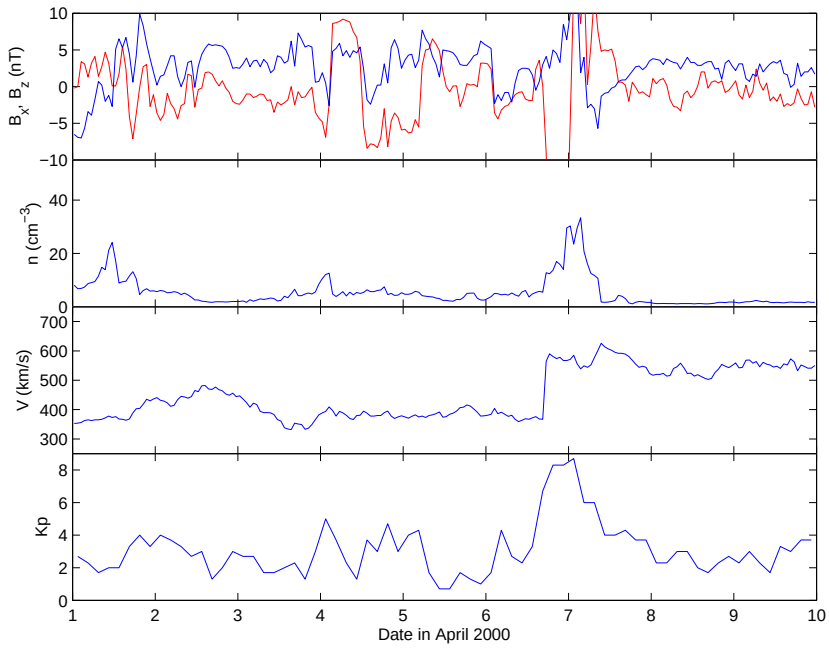

Figure 4: The solar wind magnetic field B_x (sunward component) in blue and B_z (out of the ecliptic) in red, particle density n, and velocity V during 1–10 April 2000. The geomagnetic index Kp is also shown in the bottom panel.

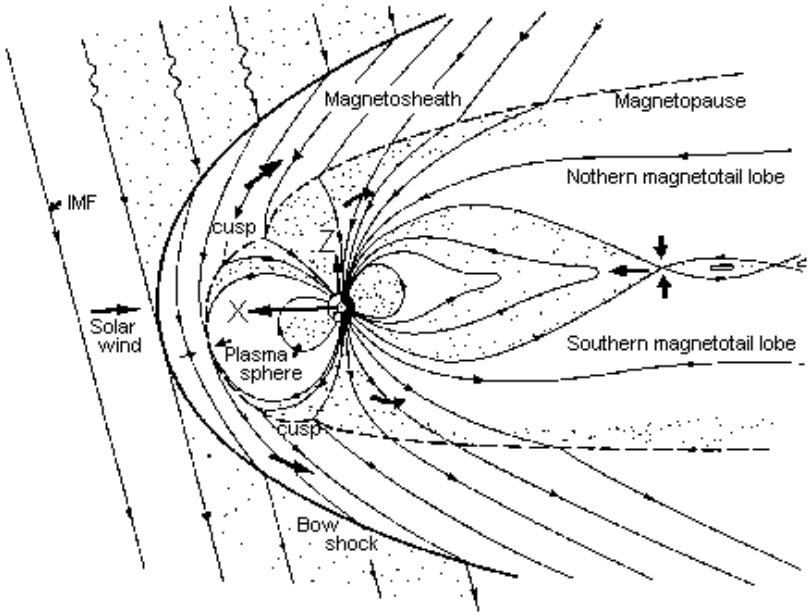

Figure 5: A cross section of the Earth and the magnetosphere (*Sonnerup*, 1985)

magnetic field strength the magnetopause moves closer to the Earth resulting in a compression of the magnetosphere and increased geomagnetic field strength.

However, through different mechanisms the solar wind plasma and magnetic field may cross the magnetopause with subsequent build-up of energy in the magnetosphere. An important mechanism is the magnetic reconnection that works highly non-linearly. Slightly simplified, the geomagnetic field on the day-side magnetopause points northward. If a structure in the solar wind contain a southward magnetic field component the solar wind magnetic field and the geomagnetic field will reconnect. This situation is illustrated in Figure 5. This will lead to that the geomagnetic field is transported towards the night side. If this situation holds for more than a couple of hours the magnetospheric tail will not be able to support the continued entry of energy. This results in instabilities, again involving magnetic reconnection, in the tail through which particles are accelerated towards the Earth. There are two major paths the particles may take, one goes into orbit around the Earth in the geomagnetic equatorial plane at about 4 Earth radii, the other follows the dipole magnetic field into the polar regions. One path forms the ring current, a current that flows westward and induced a magnetic field that is of opposite sign as that on the surface of the Earth. The *Dst* index (*Sugiura*, 1964; *Mayaud*, 1980) is derived from magnetic field measurements along the geomagnetic equator and is a measure of the strength of the ring current. The other path produces field align currents down into the ionosphere creating ionospheric currents. The AU and AL indices (*Mayaud*, 1980) measures the eastward and westward electrojets, respectively. Another auroral zone index is $AE = AU - AL$ which eliminates influence of the ring current but is less physically clear.

In Figure 6 the same period as in Figure 4 is shown but with *Dst* instead of *Kp*. The non-linear response is clearly seen as B_z turns southward in the afternoon on the 6th and *Dst* quickly reaches large negative values at the storm onset. When B_z turns northward *Dst* starts decaying back towards zero over about 2 days. The decay is caused by the diffusion of ring current particles.

There is also a small contribution from the magnetopause current, when the magnetosphere is compressed by the increased pressure, leading to a slight increase in *Dst* right before the storm onset. A model was suggested by *Burton et al.* (1975) is given by the following equations

$$
\begin{aligned}
Dst^* &= Dst - b\sqrt{p_{\mathrm{dyn}}} + c && (6)\\
p_{\mathrm{dyn}} &= mnV^2 && (7)\\
\frac{dDst^*}{dt} &= Q - \lambda Dst^* && (8)\\
Q &= \begin{cases} 0 & E_y < 0.5\mathrm{mV/m} \\ aE_y & E_y \geq 0.5\mathrm{mV/m} \end{cases} && (9)\\
E_y &= -VB_z && (10)
\end{aligned}
$$

where a, b, c, and λ are empirical constants. Dst^* is Dst corrected for the solar wind pressure, which is basically a correction for the magnetopause current. Several refinements of this model have been suggested, e.g. *O'Brien and McPherron* (2000). A slightly different approach is the use of neural networks to find the solar wind–magnetosphere coupling from the data, e.g. *Lundstedt et al.* (2002). The neural network is described by

$$
\begin{aligned}
Dst(t+1) &= \sum_{i=1}^{4} v_i x_i(t+1) + a && (11)\\
x_i(t+1) &= \tanh\left(\sum_{j=1}^{3} w_{ij} u_j(t) + \sum_{j=1}^{4} c_{ij} x_j(t) + b_i\right) && (12)\\
u_1(t) &= B_z(t) && (13)\\
u_2(t) &= n(t) && (14)\\
u_3(t) &= V(t) && (15)
\end{aligned}
$$

where v_i, w_{ij}, c_{ij}, b_i, and a are constants that are found through an iterative algorithm. Predictions from the two models are shown in Figure 6.

5 Ionosphere

The ionosphere is the ionised part of the atmosphere extending from 60 km altitude to 1000 km altitude. It can be divided into the following regions (*Hargreaves*, 1992):

Region	Altitude (km)	Electron density (m^{-3})
D	60-90	10^8-10^{10}
E	105-160	10^{11}
F1	160-180	10^{11}-10^{12}
F2	maximum at 300	10^{12}

The values are typical for daytime, however, there are both diurnal and geomagnetic modulations. Thus, the ionosphere extends from the thermosphere, through the mesopause and mesosphere, down to the stratopause.

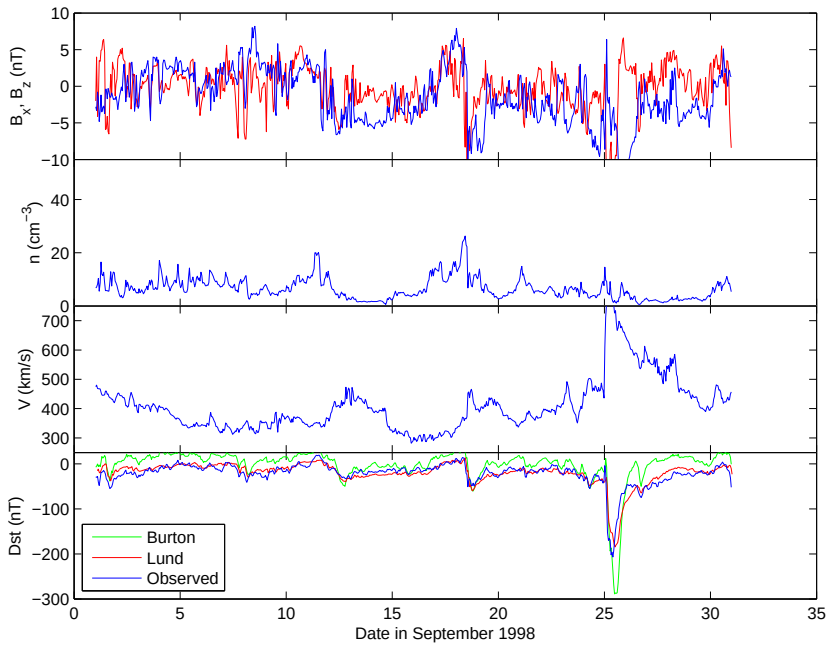

Figure 6: The solar wind magnetic field B_x (sunward component) in blue and B_z (out of the ecliptic) in red, particle density n, and velocity V during 1–31 September 1998. The geomagnetic index *Dst* is also shown in the bottom panel.

The ionosphere is created by the ionisation of gases such as N_2, O_2, and O from solar EUV radiation and energetic particles. At low to mid latitudes EUV is the main contribution to the ionisation. At high latitudes energetic particles are more important, such as auroral electrons and solar protons. The density of free electrons has a maximum at a certain height due to the decrease of atmospheric density and increase of radiation with height. The most energetic electrons ($E > 100$ keV) result in a maximum production rate at about 80 km. However, the energetic electrons also produce X-ray radiation through bremsstrahlung which has a maximum production rate at 40 km altitude. The protons reach even deeper into the atmosphere. The stopping height for a 100 MeV proton is 30 km while a 2 GeV proton can reach the ground. A major fraction of the proton energy is deposited in the last few km. The maximum electron production rate occurs at 35 km altitude for the 100 MeV protons, while the maximum production rate is below 20 km for the GeV protons. The free electrons are lost through recombination and transportation so that the electron density obeys the continuity equation

$$\frac{\partial N}{\partial t} = q - L - \nabla \cdot (N\mathbf{v}) \tag{16}$$

where N is the electron number density, q is the production rate, L loss through recombination, and $\mathbf{v}$ is the mean drift velocity. Typical electron density variation is shown in Figure 7. The particle density of the neutral atmosphere is also partially shown and it reaches 10^{12} cm^{-3} at 100 km altitude.

The F2 layer is highly variable and varies with local time, season, geomagnetic and solar activity. The F2 layer is important to HF radio communication. The existence of the F2 layer can not be explained by only considering the ionising radiation from the Sun because the electron production rate peaks at 150–170 km altitude, whereas the F2 layer is located at 200–400 km altitude. Instead the F2 layer is explained from diffusion of electrons from the lower layers. The winter and sum-

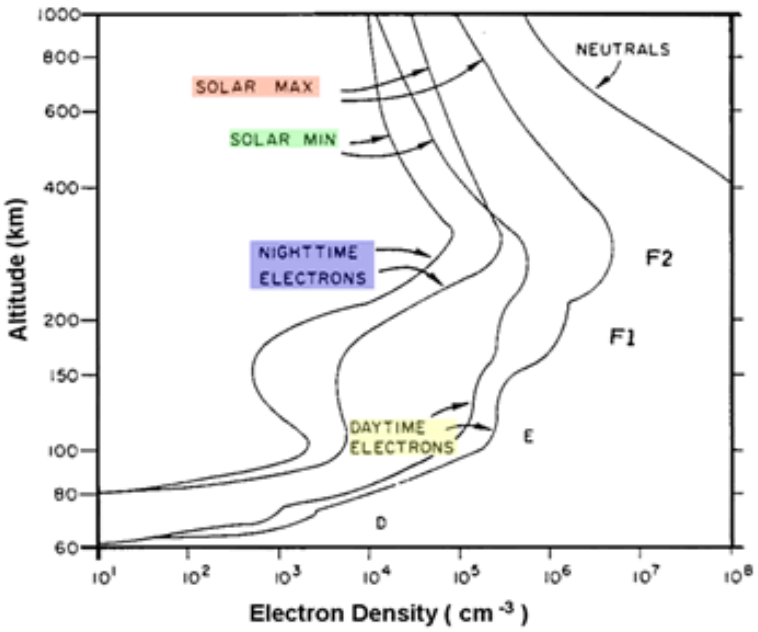

Figure 7: The electron density variation with height, solar cycle, and day. Figure from `http://www.weather.nps.navy.mil/~psguest/EMEO_online/module3/module_3_2.html`.

mer ionospheres are connected through the protonosphere. The ionosphere is the source for the protonosphere, and the protonosphere acts as a reservoir for the ionosphere. The F layers persists during the night.

Neutral winds at about 100 km altitude drives currents and creates electric fields in the E layer through collisions with charged particles moving across geomagnetic field lines. As the electrical conductivity is high along the magnetic fields lines the electric fields in the E layer also exists in the F layers causing particle drifts.

The lowest layer, the D layer, is the chemically most complex region including many different processes with positive and negative molecules. Only energetic radiation and particles reach this low and the sources for ionisation are Lyman-α, EUV, X-rays, solar energetic particles, and galactic cosmic rays, with the last being the most important at the lowest altitudes.

When neutral air flows at velocity $\mathbf{U}$ it imposes a force $\mathbf{F} = m\nu\mathbf{U}$ due to collision with collision frequency ν. With a magnetic field $\mathbf{B}$ the resulting forces become

$$\mathbf{F} + e\mathbf{v} \times \mathbf{B} - m\nu\mathbf{v} = 0. \tag{17}$$

Assuming that the wind is perpendicular to the magnetic field an electric current is generated that is perpendicular to both the wind and magnetic field. The efficiency of this dynamo is governed by the ratio between gyro frequency and collision frequency and is most efficient between 75 to 120 km. The inclination of the magnetic field will also result in a parallel wind component which will have the effect of increasing the layer height.

The plasma frequency in the ionosphere is an important parameter. It is the natural frequency at which the plasma will oscillate when an electric field is present. The plasma frequency depends on

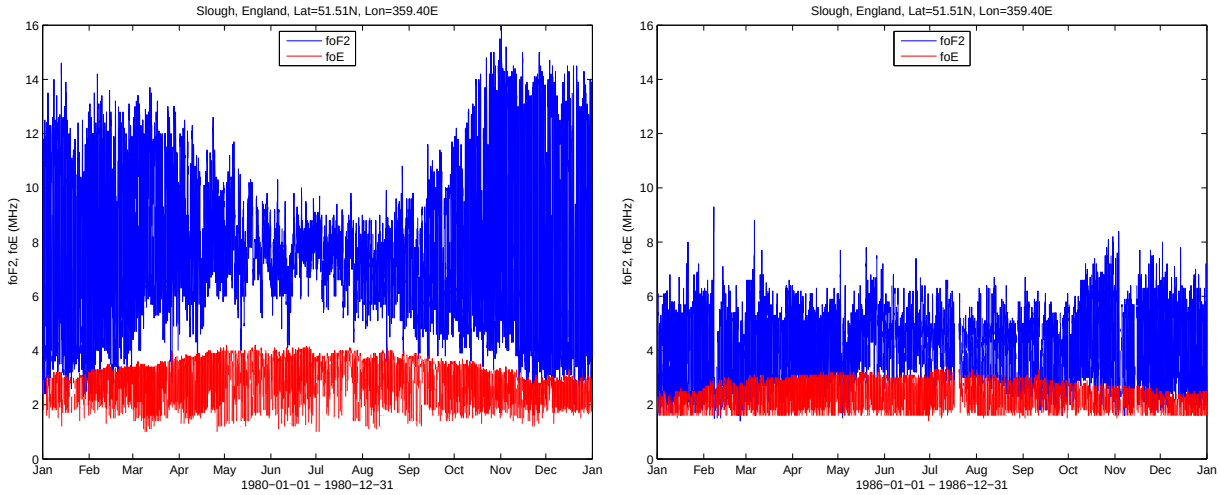

Figure 8: The figures show hourly values of the ordinary plasma frequency in the E layer (foE) and the F2 layer (foF2), respectively, for 1980 and 1986 at a northern hemisphere mid-latitude station.

the electron particle density N according to

$$\omega = \sqrt{\frac{Ne^2}{\varepsilon_0 m}} \tag{18}$$

where e is the electron charge, ε_0 is the capacitivity of vacuum, and m is the electron mass. The plasma frequency and height of the ionoshere are found using ionosonds that emits radiowaves vertically that are swept in frequency and measuring the time delay of the echo. The E- and F-layers are continuously monitored at many different sites around the world. Hourly values of the plasma frequency in F2 and E at a northern hemisphere mid-latitude station are shown in Figure 8 at sunspot maximum and sunspot minimum, respectively. The F2 layer shows a strong modulation with the sunspot cycle having the largest variation at sunspot maximum. During maximum there is also a strong seasonal variation. The E layer also show a somewhat higher plasma frequency at sunspot maximum, although the response is not as strong as in the F2 layer. There is also a seasonal dependence that is opposite to that of the F2 layer in that it show maximum variation in the summer.

The effect of the geomagnetic storm on the ionosphere can be quite different depending on the current state. In the summertime hemisphere negative storms develop, during which the charged particle density decreases, while positive storms develop in the wintertime hemisphere. There are two main sources of energy input to the ionosphere: precipitation of auroral particles and the convection of electric fields. The first source leads to increased ion density and thereby increased conductivity. The second source drives the ionosphere leading to thermospheric motion. During a storm the high-latitude heat input causes thermal expansion and establishes horizontal temperature and pressure gradients producing a divergent wind field that leads to vertical transport *Fuller-Rowell et al.* (1996). The vertical transport can explain the negative storm as the result of an increase in neutral gas composition and is known as a composition bulge (*Prölls*, 1993; *Fuller-Rowell et al.*, 1994). The local time variation can be understood as an latitudinal oscillation of the bulge, while the seasonal variation is an effect of bulge movement.

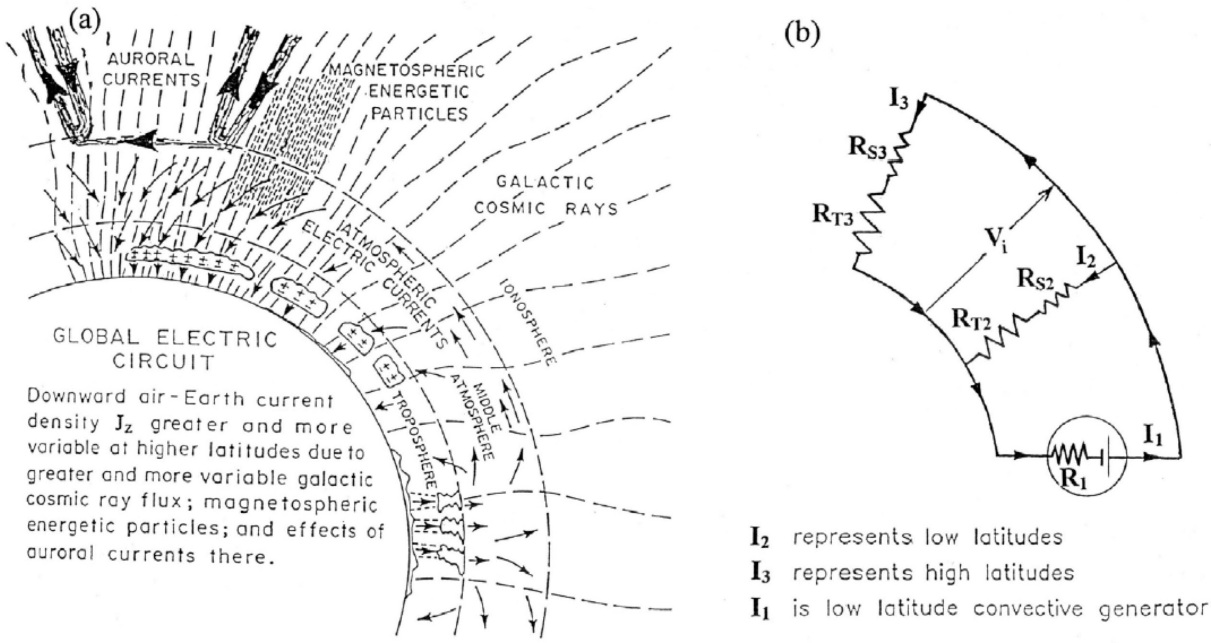

Figure 9: The global electric circuit. From *Tinsley* (2000).

The ionosphere also plays an important role in the global electric circuit (Figure 9). There are three main sources for the atmospheric currents that are related to the solar wind (*Tinsley*, 2000): 1) The galactic cosmic rays (GCR) are directly related to atmospheric conductivity for all heights in the atmosphere, thus altering both the stratospheric ($R_{S2,3}$ in Figure 9) and thermospheric ($R_{T2,3}$) resistance; 2) Precipitating relativistic electrons ($>$ 1 MeV) from the magnetosphere change the conductivity in the upper atmosphere ($R_{S2,3}$); 3) The variable polar cap potential is superimposed on the ionospheric potential V_i. We will not further discuss the modulation of the GCRs as it is covered in other WPs.

The relativistic electrons show a high degree of variability in response to the solar wind. At geostationary orbit ($\approx$ 6.7 R_e or about 45000 km) the electron flux at energies $>$ 2 MeV can increase by a factor of 10^3 in a couple of hours. The mechanism for the production of the relativistic electrons are not fully understood (*Li and Temerin*, 2001) but it is generally understood that the electrons are produced within the magnetosphere as a result of magnetospheric activity driven by the solar wind. The solar wind velocity is the single most important parameter for the electron flux with a correlation of 40–60% (*Vassiliadis et al.*, 2002). The electron flux is reach its peak value about 1–2 days after a solar wind velocity increase associated with the high speed streams from coronal holes. The duration of the flux enhancement is about 3 days at geosynchronous orbit and increases to 6 days at 4 R_e in the equatorial plane (*Vassiliadis et al.*, 2002). As the geomagnetic field lines converge towards the poles it means that the electrons reach much lower altitudes in the auroral zone.

6 Time scales of variability

When discussing the physical mechanisms that operate between the various systems it is interesting to study the typical time scales of variability.

6.1 Solar wind

As seen in Section 3 the solar wind displays a high degree of variability. This variability is caused by three main sources at the Sun: coronal mass ejections (CME), coronal holes (CH), and coronal streamers (CS). As all these phenomena are correlated with the sunspot number there will be a variation in the solar wind that follows the sunspot number cycle. In the following we study the solar wind variability for the different phases of the sunspot number cycle.

6.2 Magnetospheric activity

Forming temporal averages of *Dst* over Carrington rotations ($\sim$ 27 days) and applying the continuos wavelet transform gives the power spectrum shown in Figure 10 (middle panel). The dominating feature here is the 11 year period. The top panel of Figure 10 shows the power spectrum of the sunspot number *Rz*. Both show the 11-year period although there is no physical relation between *Rz* and *Dst*. There is some weak power around 0.5 years in *Dst* that is caused by the tilt of the geomagnetic dipole and the Earth's orbit around the Sun favouring solar wind entry twice per year (*Russell and McPherron*, 1973). There are no other variations with clear periodicity. The wavelet coherence between *Rz* and *Dst* is shown in the bottom panel of Figure 10. The strongest correlation is found, as expected, around 11 years. However, there is a shifting of the phase with a 180° phase difference in 1965 turning towards 90° in 2000, indicative of the lack of physical connection between *Rz* and *Dst*.

Kp displays a similar power spectrum as *Dst* although there are also clear differences. *Dst* has strong and significant power close to 11 years for the whole period studied. *Kp* has a peak in power around 9 years in 1980 and drifts towards 11 years in 2000 (Figure 11, top panel). The two indices *Kp* and *Dst* are both global measures of magnetospheric activity, however, they capture variations for different regimes. *Dst* measures the deviation of the (geomagnetic) equatorial variation and is basically an indicator for the ring current. *Kp* measures variations of the magnetic field at mid-latitude and contain several different sources. The wavelet coherence between the two indices for Carrington averages is shown in Figure 11 (bottom panel). It is seen that there is no clear correlation between the two indices around the 11-year period, while there is strong correlation at the semi-annual level.

6.3 Coupling between systems

There are considerable coupled variability in the solar wind, magnetosphere and ionosphere on very short time scales (minutes) and that may last for several days. The coupling is also often non-linear

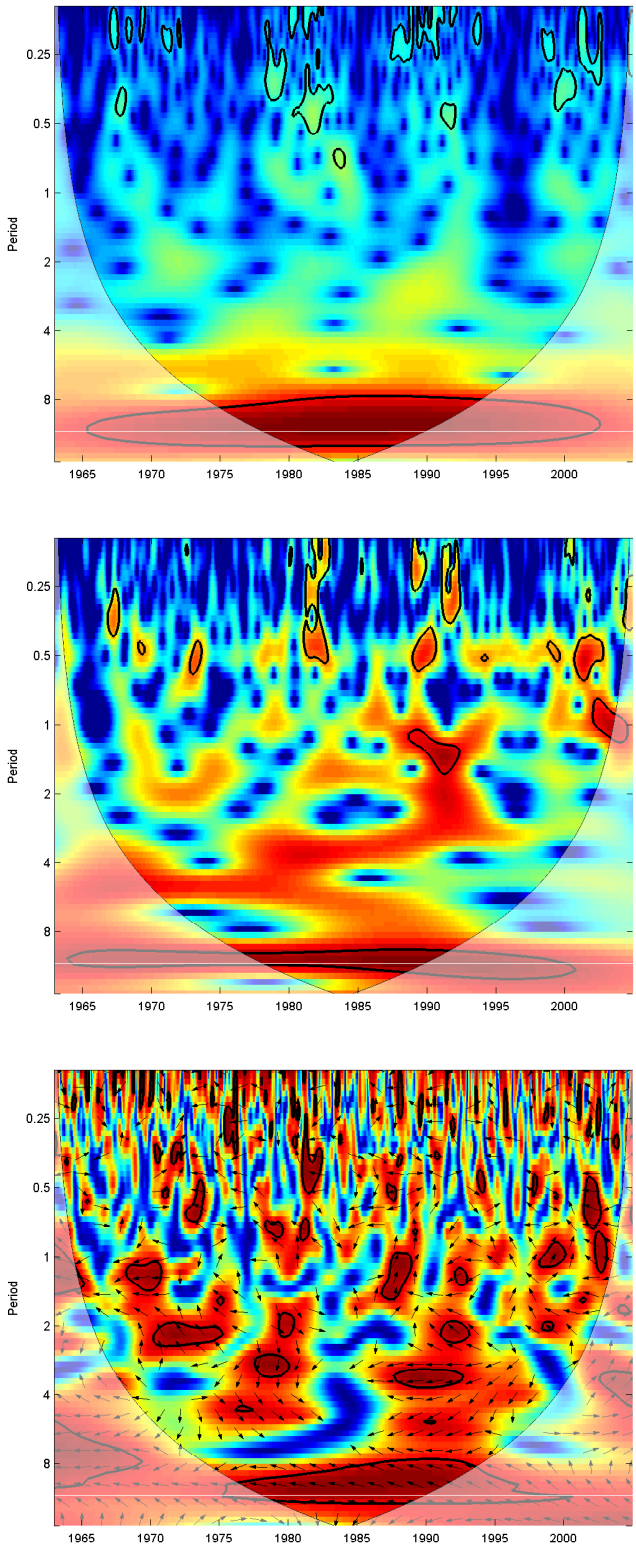

Figure 10: Wavelet power spectrum of *Dst* averaged over Carrington rotations. The white horizontal line marks a period of 11 years.

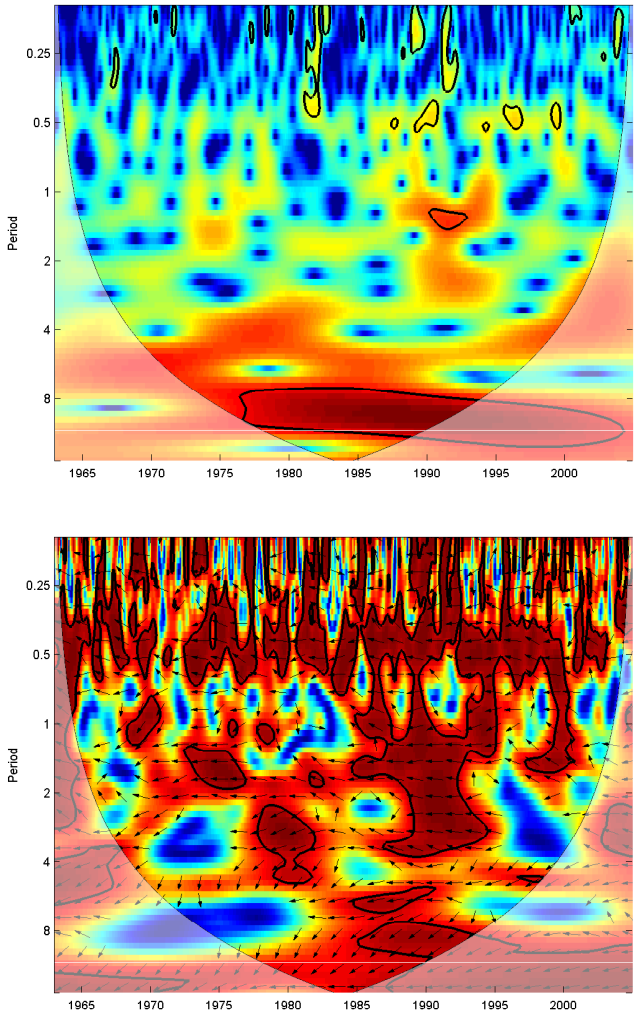

Figure 11: Wavelet power spectrum of Kp averaged over Carrington rotations. The white horizontal line marks a period of 11 years.

as is very clear from the north-south asymmetric dependence on solar wind B_z. In the study by *Boberg and Lundstedt* (2002) a correlation was found by the solar wind electric field and the North Atlantic Oscillation (NAO) index. The NAO variability is the result of a few proposed mechanisms: 1) eddy-mean flow interactions internal to the atmosphere, 2) stratospheric/tropospheric planetary wave interactions, 3) remote forcing from the tropics, and 4) thermal coupling with the ocean mixed layer. Thus, the solar wind could couple to the atmosphere via mechanism 2 through the entry of energy into the magnetsphere/ionosphere that drive stratospheric/tropospheric planetary waves.

References

Baumjohann, W., and G. Haerendel, Entry and dissipation of energy in the Earth's magnetosphere, in *Space Astronomy & Solar System Exploration: Proceeding of Summer School held at Alpbach, Austria, 29 July – 8 August, 1986, ESA SP-268*, pp. 121–130, ESA, 1987.

Boberg, F., and H. Lundstedt, Solar wind variations related to fluctuations of the North Atlantic Oscillation, *Geophysical Research Letters*, *29*(15), doi:10.1029/2002GL014903, 2002.

Burlaga, L. F., *Interplanetary magnetohydrodynamics*, Oxford University Press, 1995.

Burton, R. K., R. L. McPherron, and C. T. Russell, An empirical relationship between interplanetary conditions and *Dst*, *Journal of Geophysical Research*, *80*(31), 4204–4214, 1975.

Fuller-Rowell, T. J., M. V. Codrescu, R. J. Moffett, and S. Quegan, Response of the thermosphere and ionosphere to geomagnetic storms, *Journal of Geophysical Research*, *99*, 3893–3914, 1994.

Fuller-Rowell, T. J., M. V. Codrescu, H. Rishbeth, R. J. Moffett, and S. Quegan, On the seasonal response of the thermosphere and ionosphere to geomagnetic storms, *Journal of Geophysical Research*, *101*(A2), 2343–2353, 1996.

Hargreaves, J. K., *The solar-terrestrial environment*, Cambridge University Press, 1992.

Li, X., and M. A. Temerin, The electron radiation belt, *Space Science Review*, *95*(1–2), 569–580, 2001.

Lockwood, M., *Solar outputs, their variations and their effects on Earth*, pp. 109–306, Saas-Fee Aadvanced Course 34 2004, Springer-Verlag Berlin Heidelberg, 2005.

Lundstedt, H., H. Gleisner, and P. Wintoft, Operational forecasts of the geomagnetic *Dst* index, *Geophysical Research Letters*, *29*(24), 34–1–34–4, doi:10.1029/2002GL016151, 2002.

Mayaud, P. N., Derivation, meaning, and use of geomagnetic indices, *Geophysical Monograph Series,* American Geophysical Union, 1980.

O'Brien, T. P., and R. L. McPherron, Forecasting the ring current index *Dst* in real time, *Journal of Atmospheric and Solar-Terrestrial Physics*, *620*, 1295–1299, 2000.

Prölls, G. W., On explaining the local time variation of ionospheric storm effects, *Annales Geophysicae*, *110*, 1, 1993.

Russell, C. T., and R. L. McPherron, Semiannual variation of geomagnetic activity, *Journal of Geophysical Research*, *78*(1), 92–108, 1973.

Sonnerup, B. U. O., Solar wind interaction with planetary magnetic fields, in *Proc. ESA Workshop on Future Mission in Solar, Heliospheric & Space Plasma Physics, Garmisch-Partenkirchen, Germany, 30 April – 3 May 1985, ESA SP-235*, pp. 53–64, 1985.

Sugiura, M., Hourly values of equatorial *Dst* for the IGY, *Annals of the International Geophysical Year*, *35*, 9–45, 1964.

Tinsley, B. A., Influence of solar wind on the global electric circuit, and inferred effects on cloud microphysics, temperature, and dynamics in the troposphere, *Space Science Reviews*, *94*, 231–258, 2000.

Vassiliadis, D., A. J. Klimas, S. G. Kanekal, D. N. Baker, and R. S. Weigel, Long-term-average, solar cycle, and seasonal response of magnetospheric energetic electrons to the solar wind speed, *Journal of Geophysical Research*, *107*(A11), SMP 22–1–17, doi:10.1029/2001JA000506, 2002.

Zhao, X., and J. T. Hoeksema, Unique determination of model coronal magnetic fields using photospheric observations, *Solar Physics*, *143*, 41–48, 1993.